
Supervised Distributional Reduction via Optimal Transport and Dependence Maximization

Sai-Aakash Ramesh^{1*} Archit Sood¹ Andrew Corbett¹ Tim Dodwell^{1,2}
¹digiLab, UK ²University of Bristol, UK

Abstract

Learning representations that capture both intrinsic data geometry and target-relevant structure remains a fundamental challenge, particularly in settings where data reduction must balance compression with predictive fidelity. While distributional reduction-encompassing joint clustering and dimensionality reduction-offers a principled way to summarize data, its supervised variants remain relatively under-explored, despite the importance of retaining task-relevant signal for downstream prediction and decision-making. We propose Supervised Distributional Reduction (SDR), an algorithm for learning target-aware representations by combining optimal transport with explicit dependence maximization. SDR builds on the Fused Gromov-Wasserstein (FGW) objective to align the relational structure of the input distribution with a set of representative points, while augmenting it with a direct dependence term that encourages the learned embeddings to capture predictive signal more explicitly. This results in compact representations that reflect both geometric structure and supervision. Beyond representation learning, SDR naturally induces a data-dependent, non-stationary geometry that can be leveraged for settings such as Gaussian Process (GP) modelling. By redefining distances through target-aware distributional alignment, SDR enables the construction of adaptive kernels that respond to local variations in both data geometry and supervision, offering an optimal transport-based perspective on non-stationary kernel design.

1 Introduction

Optimal Transport (OT) provides a principled framework for comparing probability distributions, with Gromov-Wasserstein (GW) [Peyré et al., 2016] enabling alignment across heterogeneous spaces by matching relational structure. Building on this, Distributional Reduction (DistR) [Assel et al., 2025] learns a low-dimensional set of representative points that preserves the geometry of a dataset, providing a framework for unifying clustering and dimensionality reduction. However, existing distributional reduction methods are largely unsupervised, which can lead to representations that fail to retain task-relevant information and lack a clear mechanism for out-of-sample generalization. This prevents these methods from being used for downstream prediction tasks.

We address these limitations by proposing Supervised Distributional Reduction (SDR), a framework for learning target-aware latent representations by combining optimal transport with explicit dependence maximization. SDR builds on the Fused Gromov-Wasserstein (FGW) objective [Vayer et al., 2018] to align the relational structure of the input distribution with representative points, while incorporating supervision. Crucially, rather than relying solely on the coupling matrix—where supervision is mediated indirectly and may be diluted by structural constraints—we augment the objective with a direct representation-level dependence term based on Centered Kernel Alignment (CKA). This enables explicit alignment between embeddings and targets while preserving intrinsic data geometry.

*Correspondence to Sai-Aakash Ramesh: <sai-aakash.ramesh@digiLab.ai>

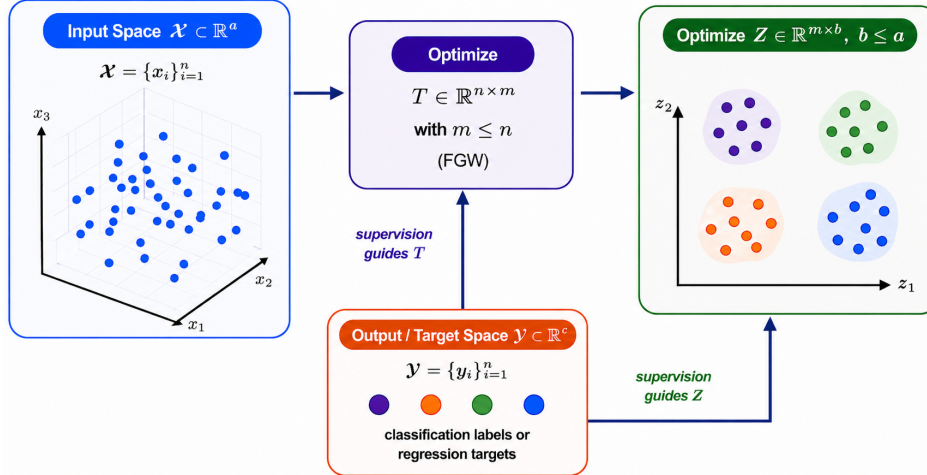


Figure 1: Supervised Distributional Reduction (SDR) with Fused Gromov-Wasserstein OT formulation and explicit dependence maximization for target-aware distributional reduction.

Beyond representation learning, SDR induces a data-dependent, non-stationary geometry that can be exploited for kernel learning. By constraining embeddings to admit an approximate kernel-based out-of-sample extension, we obtain a stable projection mechanism for unseen data. This allows SDR to define adaptive covariance functions for Gaussian Processes (GPs), where the learned geometry translates into non-stationary kernel behaviour that responds to both structure and supervision in the data.

1.1 Contributions

We make the following contributions in this work:

1. **Supervised distributional reduction via OT and dependence maximization:** We propose SDR, an algorithm that combines OT-based alignment with explicit dependence maximization to learn compact, target-aware representations that preserve both geometry and predictive signal.
2. **Out-of-sample extension via RKHS projection with applications to GPs:** We formulate the mapping from inputs to embeddings as a regularized kernel ridge regression problem, yielding an out-of-sample transformation map that allows SDR to be used as part of predictive pipelines and for non-stationary kernel construction in GPs.

2 Related Work

2.1 Supervised Dimensionality Reduction and Clustering

Supervised dimensionality reduction (DR) methods incorporate label information to learn representations that are more discriminative for downstream tasks. Classical approaches such as Linear Discriminant Analysis (LDA) [Fisher, 1936] maximize class separability through linear projections, while metric learning methods, including Neighbourhood Components Analysis (NCA) [Goldberger et al., 2004] and Large Margin Nearest Neighbour (LMNN) [Weinberger et al., 2005], shape the embedding space using supervised distance objectives. Extensions of unsupervised DR techniques have also been proposed in supervised settings; for instance, Supervised UMAP [McInnes et al., 2020] integrates label information to guide the preservation of local structure in a target-aware manner. In parallel, dependence-based approaches maximize statistical dependence between representations and targets. For example, using the Hilbert Schmidt Independence Criterion (HSIC) [Gretton et al., 2007] in conjunction with PCA gives rise to a version of Supervised PCA [Barshan et al., 2011]. On the other hand, supervised and semi-supervised clustering methods introduce constraints such as must-link and cannot-link pairs to guide cluster formation [Wagstaff et al., 2001]. Xing et al. [2002]

suggest providing supervision in the form of distances (similarities) for metric-informed clustering. Despite these advances, most approaches either focus solely on embedding or clustering, or rely on heuristic combinations of the two, lacking a unified formulation that captures both aspects at the distributional level.

2.2 Optimal Transport, GW/FGW, and Distributional Reduction

Optimal transport (OT) provides a principled framework for comparing probability distributions by minimizing the cost of transporting probability mass between them [Monge, 1781, Kantorovitch, 1958]. Beyond classical Wasserstein distances, Gromov–Wasserstein (GW) extends OT to settings where only relational information, such as pairwise distances, is available, enabling comparisons across heterogeneous spaces [Peyré et al., 2016]. The Fused Gromov–Wasserstein (FGW) formulation further combines feature-level and structural alignment by integrating Wasserstein and GW objectives into a single framework [Vayer et al., 2018]. These formulations provide a natural mechanism for geometry-aware representation learning. Building on these ideas, OT-based approaches have been proposed for distributional summarization, including Wasserstein barycenters [Cuturi and Doucet, 2014] and reduced-support approximations [Forrow et al., 2019]. Methods such as DistR [Assel et al., 2025] leverage GW to jointly perform clustering and dimensionality reduction by learning a reduced set of representative points that preserve dataset geometry. However, these approaches are largely unsupervised and do not explicitly incorporate target information during the reduction process.

SDR builds on this line of work by integrating supervision directly into the distributional reduction objective, enabling the learning of compact representations that are both geometry-preserving and target-aware.

3 Method

3.1 Distributional Reduction with OT

Distributional Reduction (DistR) [Assel et al., 2025] formulates joint clustering and DR as an optimal transport problem between the original dataset and a reduced set of representative embeddings. Given input data $X \in \mathbb{R}^{n \times d}$, DistR seeks a reduced representation $Z \in \mathbb{R}^{m \times p}$ with $m \leq n$ and $p \leq d$ by solving a Gromov–Wasserstein (GW) OT problem between their respective metric structures.

Let C and \bar{C} denote pairwise distance matrices in the input and embedding spaces respectively and \mathbf{h}_X denote the weight vector typically assumed to be uniform, that is $\mathbf{h}_X = \frac{1}{n} \mathbf{1}_n$. DistR solves:

$$\min_{\substack{\mathbf{T} \in \mathcal{U}(\mathbf{h}_X) \\ \mathbf{Z} \in \mathbb{R}^{m \times p} \\ \mathbf{h}_Z \in \Sigma_m}} \sum_{ijkl} L_u(C_{ij}, \bar{C}_{kl}) T_{ik} T_{jl} \quad (\text{DistR})$$

where T is a transport plan in $\mathcal{U}(\mathbf{h}_X) = \{T \in \mathbb{R}_+^{n \times m} : T \mathbf{1}_m = \mathbf{h}_X\}$ between the input and reduced representations, and L_u is an unsupervised, structural loss function comparing pairwise distances. The problem is optimized via alternating minimization over T and Z , where T is computed using standard GW solvers and Z is updated using gradient-based methods. When $m < n$, this yields a reduced set of representative points weighted non-uniformly with h_Z , unifying clustering and dimensionality reduction within a single framework.

3.2 Supervised Distributional Reduction

In this section, we extend the Distributional Reduction Algorithm to the supervised setting. SDR optimizes a single unified objective over (Z, T) , where alternating minimization is used to handle the non-convex coupling between the variables. The SDR objective solves the following two subproblems in the T and Z update steps:

- T -step: Solving a Fused-Gromov Wasserstein (FGW) alignment subproblem for T
- Z -step: Optimizing a supervised representation subproblem for Z

3.2.1 Optimal Transport with Supervised FGW

The Fused Gromov-Wasserstein (FGW) [Vayer et al., 2018] objective is formulated as follows:

$$FGW_\alpha(\mathbf{C}, \bar{\mathbf{C}}, \mathbf{h}, \bar{\mathbf{h}}; \mathbf{T}) = (1 - \alpha) \sum_{ij} L_s(f_i, f_j) T_{ij} + \alpha \sum_{ijkl} L_u(C_{ij}, \bar{C}_{kl}) T_{ik} T_{jl} \quad (\text{FGW})$$

where, f_i and f_j are features of a point x_i in the input space and a point z_j in the embedding space respectively, L_s is a feature-level loss function and α is a hyperparameter that controls the magnitudes of both these losses. In this work, we make a specific choice for the features. We set these features to be the target values (regression targets/class labels) present in a dataset. The proposed FGW-based objective for the supervised alignment subproblem is as follows:

$$FGW_\alpha(C, \bar{C}, Y, h, \bar{h}; T) = \min_{T \in \mathcal{U}(h, \bar{h})} (1 - \alpha) \sum_{ij} L_s(y_i, g_j) T_{ij} + \alpha \sum_{ijkl} L_u(C_{ij}, \bar{C}_{kl}) T_{ik} T_{jl} \quad (1)$$

where y_i, g_j are the target values corresponding to x_i and z_j and they replace f_i, f_j in the original FGW objective respectively. This objective is intractable in conventional ML settings since g_j (prototype targets) may not be available (this might not apply to graphs since for two graphs in question, both graphs can have node-level labels/features available). That makes $\mathbf{G} = (g_1, g_2, \dots, g_m)$, additional parameters to be optimized as part of the objective. For notational convenience, we make the summation variables explicit, abbreviate the GW loss and rewrite the objective in Eqn.(1) as follows:

$$\mathcal{J}(T, Z, G) = (1 - \alpha) \sum_{i=1}^n \sum_{j=1}^m L_s(y_i, g_j) T_{ij} + \alpha GW(Z; T) \quad (\text{S-FGW})$$

The key insight is that we can analytically eliminate the prototype targets g_j from the S-FGW objective by solving for a partially minimized objective as described in Remark 3.1. Lemma 3.2 shows how we can eliminate prototype targets in closed form by leveraging the Bregman barycentric structure yielding a tractable objective that depends only on (T, Z) .

Remark 3.1 (Elimination of Prototype Targets by Partial Minimization).

The supervised FGW objective is separable in the prototype targets $G = \{g\}_{j=1}^m$. For fixed T and Z , each g_j can therefore be optimized independently as

$$g_j^*(T) = \arg \min_{g \in \mathcal{G}} \sum_{i=1}^n L_s(y_i, g) T_{ij} \quad (2)$$

assuming \mathcal{G} is compact and $L_s(y, g)$ is lower semicontinuous for the minimizer to exist. Substituting these minimizers yields an equivalent reduced objective depending only on (T, Z) ,

$$\min_{T, Z, G} \mathcal{J}(T, Z, G) = \min_{T, Z} \mathcal{J}(T, Z, G^*(T)) \quad (3)$$

Lemma 3.2 (Optimal Prototypes for Bregman Losses; adapted from Banerjee et al. [2005] and Nielsen and Nock [2009]).

Let L_s be a Bregman divergence generated by a differentiable, strictly convex function ϕ on a convex domain $\mathcal{G} \subseteq \mathbb{R}^c$ and let $\pi_j := \sum_{i=1}^n T_{ij} > 0$. Then the optimal prototype target satisfies:

$$g_j^*(T) = \begin{cases} (\nabla \phi)^{-1} \left(\frac{1}{\pi_j} \sum_{i=1}^n T_{ij} \nabla \phi(y_i) \right), & (\text{dual-form}) \\ \frac{1}{\pi_j} \sum_{i=1}^n T_{ij} y_i, & (\text{primal-form}) \end{cases} \quad (4)$$

Corollary 3.3 (Prototype targets for Squared Loss and Cross Entropy Loss).

For standard supervised losses used in practice particularly the L2-loss for regression and the cross-entropy loss for classification, the optimal prototype targets reduce to:

$$g_j^*(T) = \frac{\sum_{i=1}^n T_{ij} y_i}{\sum_{i=1}^n T_{ij}} = \frac{1}{\pi_j} \sum_{i=1}^n T_{ij} y_i \quad (5)$$

The proof for Lemma 3.2 is provided in Appendix A while the derivation for Corollary 3.3 using Lemma 3.2 is provided in Appendix B. Substituting $g_j^*(T)$ yields a reduced objective depending only on (T, Z) , which we refer to as the barycentric supervised FGW (BS-FGW) objective.

$$\mathcal{J}(T, Z) = (1 - \alpha) \sum_{i=1}^n \sum_{j=1}^m L_s(y_i, g_j^*(T)) T_{ij} + \alpha GW(Z; T) \quad (\text{BSFGW})$$

For the BSFGW objective we will solve a semi-relaxed version of this objective to allow for re-weighting of the embeddings along with the optimization of coupling matrix T inheriting the same strategy from DistR. The optimization of h_Z will be through the semi-relaxed version of the BSFGW objective [Vincent-Cuaz et al., 2022]. The semi-relaxed BSFGW objective is formulated as:

$$\mathbf{T}^* = \min_{T \in \mathcal{U}(h_X)} (1 - \alpha) \sum_{i=1}^n \sum_{j=1}^m L_s(y_i, g_j^*(T)) T_{ij} + \alpha GW(Z; T) \quad (\text{srBSFGW})$$

3.2.2 Supervised Representation Optimization

The DistR objective is elegant in the sense that it uses the same GW loss to optimize for both Z and T . However, this is not so straightforward in the supervised setting. The BSFGW objective introduces supervision indirectly via T , and this creates a supervision bottleneck as described in the following remark.

Remark 3.4. *The partially minimized BSFGW objective exhibits two key limitations:*

- (i) **No direct supervision in representation updates:** For fixed T , the supervised term does not depend on Z , and the representation update is governed solely by the geometric term.
- (ii) **Attenuated supervision under joint optimization:** When optimizing jointly, supervision influences Z only through the sensitivity of the optimal coupling $T^*(Z)$ with respect to Z , which can lead to weak gradients when $T^*(Z)$ is locally insensitive to Z or when dominated by structural constraints.

In regimes where $T^*(Z)$ is dominated by structural constraints or is locally insensitive to Z , the supervised gradient on Z is attenuated leading to weak alignment between Z and Y . Theoretical justification for Remark 3.4 is provided in Appendix C.1.

To address this, we introduce a direct dependence-maximization term, which complements FGW by providing strong gradients on Z . We inject an explicit supervision term using a normalized version of the HSIC score called the **Centred Kernel Alignment (CKA)** [Kornblith et al., 2019] which is defined over two variables Z and Y as:

$$\text{CKA}(Z, Y) = \frac{\langle K_Z, K_Y \rangle_{\mathcal{F}}}{\|K_Z\|_{\mathcal{F}} \|K_Y\|_{\mathcal{F}}} \quad (\text{CKA})$$

where, K_Z and K_Y are kernel matrices over Z and Y respectively and $\|\cdot\|_{\mathcal{F}}$ denotes the Frobenius norm. We use CKA as a dependence maximization objective to directly align representations with targets, building on prior work that employs similar dependence-based criteria (e.g., HSIC) for supervised dimensionality reduction [Barshan et al., 2011, Gretton et al., 2007, Zhang et al., 2017]. Unlike pointwise losses, CKA operates at the representation level and captures global dependence consistent with the global, structure-preserving perspective of OT. The normalized range of CKA makes it interpretable and offers easier tuning for the hyperparameter η when combined with the GW loss in the SDR objective. For $m < n$, we compute CKA using a coupling-induced projection $K_{\tilde{Y}\tilde{Y}} = T^\top K_{YY} T$, which defines target similarities in the reduced space. This can be thought of as a transport-weighted kernel compression technique that allows CKA computation in the prototype space. In Appendix C.2 we provide some empirical evidence on the effect of the additional CKA term compared to the vanilla BSFGW objective. Combining the CKA term with the BSFGW objective, the joint optimization objective for \mathbf{Z} and \mathbf{T} is given by:

$$\mathcal{J}_{\text{SDR}}(Z, T, h_Z) = (1 - \alpha) \sum_{i=1}^n \sum_{j=1}^m L_s(y_i, g_j^*(T)) T_{ij} + \alpha \text{GW}(Z; T) - \eta \text{CKA}(Z, \tilde{Y}) \quad (\text{SDR})$$

By minimizing the negative of the CKA term we maximize the correlation between the variables Z and \tilde{Y} with η being a hyperparameter that can be tuned to increase/decrease the effect of the CKA term in the objective. We minimize \mathcal{J}_{SDR} to obtain the embeddings Z , coupling matrix T and the weighting h_Z of the embeddings:

$$\mathbf{Z}^*, \mathbf{T}^*, \mathbf{h}_Z^* = \min_{\substack{Z \in \mathbb{R}^{m \times p} \\ h_Z \in \Sigma_m \\ T \in \mathcal{U}(\mathbf{h}_X)}} \mathcal{J}_{\text{SDR}}(Z, T, h_Z) \quad (6)$$

We adopt an inexact (surrogate) block coordinate descent scheme w.r.t T to solve for the SDR objective. In particular, the T-step optimizes the srBSFGW objective ignoring the CKA term. This design is intentional for two reasons: (i) including the CKA term in the transport subproblem would break the structure required for efficient OT solvers and introduce high-order, normalized dependencies on T ; and (ii) CKA is designed to provide direct supervision on the representation Z , addressing the supervision bottleneck without requiring gradients through the transport solver. The srBSFGW objective is solved using a CG solver [Jaggi [2013], Vincent-Cuaz et al. [2022]] to optimize for T which will consequently recover $h_Z = T^\top \mathbf{1}_n$ as the second marginal. The Z -step optimizes the sum of the GW and CKA terms using SGD optimizers like Adam [Kingma and Ba, 2017]. It is worth noting that SDR inherits the same runtime complexity as DistR which is $\mathcal{O}(nm^2 + mn^2)$ according to Proposition 1 in [Peyré et al., 2016].

4 Mapping Estimation for SDR

While SDR learns embeddings that are strongly aligned with targets, these representations are not guaranteed to admit a functional mapping from the input space. This lack of an explicit mapping prevents SDR from being used in downstream predictive settings, where embeddings for unseen inputs must be computed. To enable out-of-sample generalization, we therefore seek embeddings Z that are not only target-aware but also approximately representable as a kernel map from the inputs. Concretely, we enforce that Z lies close to the image of a function in the RKHS induced by a kernel K , leading to the approximation $Z \approx KL$, where L parametrizes the mapping. This perspective allows us to learn embeddings that retain the advantages of SDR while ensuring they can be consistently extended to unseen data. Consequently, this allows SDR to be used as part of a predictive pipeline.

We take inspiration from Perrot et al. [2016] to propose a modified objective which augments the original SDR objective with a projection-consistency term as follows

$$\mathcal{J}_{\text{SDR-OOS}}(Z, T, L) = \mathcal{J}_{\text{SDR}}(Z, T) + \frac{\mu}{2} \|TZ - KL\|_F^2 + \frac{\lambda_L}{2} \text{Tr}(L^\top KL) \quad (\text{SDR-OOS})$$

where, $K \in \mathbb{R}^{n \times n}$ is the covariance matrix of the training points X according to a kernel function (typically RBF), $L \in \mathbb{R}^{n \times p}$ is the transformation map, and λ_L is a regularization parameter for the transformation map L with the last term defining the RKHS norm of L . μ is a regularization parameter for Z that forces Z to lie close to the RKHS representable set of the kernel function used to compute K .

Note that the L -subproblem is a quadratic function in L . The L -subproblem therefore is the sum of a least-squares term with an L2-regularizer. Since $\lambda_L > 0$, the Hessian with respect to L is positive definite. Hence, the L -subproblem is strongly convex and admits a unique minimizer. The closed form for this unique minimizer is given by

$$L^* = (\mu K^T K + \lambda_L I)^{-1} \mu K^T T Z \quad (7)$$

Estimating the OOS map reduces to vector-valued kernel ridge regression from the input kernel K to the SDR representation, providing a stable and well-posed projection operator for unseen points. Without loss of generality, we set $\mu = 1$ since it can be absorbed into the regularization parameter λ_L . To provide intuition and simplify exposition, we focus on the pure dimensionality reduction case ($p < d, m = n$). For this case, in the absence of entropic regularization, the optimal coupling matrix is a permutation matrix under uniform marginals with strong structural and target alignment. With K being a symmetric matrix, the expression for L^* simplifies to the usual kernel ridge form,

$$L^* = (K + \lambda_L I)^{-1} Z \quad (8)$$

The SDR-OOS objective can be similarly solved with BCD by having three alternating updates for T, Z and L . After updating L , we perform a relaxation step that moves Z toward the RKHS-representable set defined by the current projection KL^* , while also retaining flexibility introduced by the SDR objective. This update can be written down as follows:

$$Z' = (1 - \beta)Z + \beta KL^* \quad (9)$$

where β controls the trade-off between preserving target-aligned structure in the learned embeddings and enforcing consistency with the RKHS projection for improved generalization. The soft update can be extended to the $m \neq n$ (for SDR typically $m < n$) case analogously as,

$$Z' = (I + \beta T^T T)^{-1} (Z + \beta T^T KL^*) \quad (10)$$

4.1 SDR for Non-Stationary Kernel Construction in GPs

Gaussian Processes (GPs) with stationary kernels are limited in their ability to capture input-dependent variations in function behaviour. A common approach to address this is Deep Kernel Learning (DKL) [Wilson et al., 2016], where a neural network is jointly trained with the GP to learn a feature representation that induces non-stationarity. While effective, this approach relies on parametric feature extractors and joint optimization of the network parameters and the GP hyperparameters, which can be sensitive to initialization and challenging to train in low-data regimes. Deep Gaussian

Processes (DGPs) [Damianou and Lawrence, 2013] provide another way to introduce non-stationarity by modelling each intermediate representation in a deep belief network with a data-driven GP prior but are expensive to train and converge much slower in practice.

SDR provides an alternative mechanism for constructing non-stationary kernels by learning target-aware representations through optimal transport and dependence maximization in the pure DR setting ($p < d, m = n$). When a stationary kernel (e.g., RBF) is applied in the SDR embedding space, the induced kernel in the original input space becomes data-dependent and non-stationary. The GP prior with an SDR induced kernel can be written as,

$$f \sim \mathcal{GP}(m(\cdot), \psi(z(\cdot), z(\cdot))) \quad (\text{SDR-GP})$$

where, m is a mean function, ψ is a stationary kernel like the RBF. The mapping $z(\cdot)$ uses the projection map L optimized by the SDR-OOS objective to project an unseen point x^* and is given by,

$$z(x^*) = K(x^*, X)L \quad (11)$$

where K is also a stationary kernel like RBF acting in the input space.

Unlike DKL, this approach decouples representation learning from GP training and leverages a target-aware objective that explicitly aligns representations with targets. The SDR-OOS objective equipped with a projection map allows SDR to serve as a plug-in feature extractor for GPs, providing a non-parametric route to non-stationary kernel design grounded in distributional alignment.

5 Experiments

5.1 Distributional Reduction Benchmarks

To assess the effect of incorporating supervision, we follow the evaluation protocol used in prior joint clustering and dimensionality reduction methods, particularly DistR. We use three classification datasets namely: COIL-20 [Nene et al., 1996], Fashion-MNIST [Xiao et al., 2017] and SNAREseq [Chen et al., 2019] for the experiments in this subsection. Further details of the datasets are provided in Appendix E. Since label information Y is explicitly used during optimization, these metrics do not reflect unsupervised clustering performance, but rather the extent to which the learned representation captures target-relevant structure. Accordingly, we report homogeneity score, k-means normalized mutual information (NMI), and silhouette score, interpreting them as measures of label consistency and semantic coherence of the embeddings.

We compare SDR against DistR, Cluster-then-DR, and DR-then-Cluster to isolate the effect of incorporating supervision within a distributional reduction pipeline. The results of this benchmark are shown in Figure 2, with runtimes plotted in Figure 3. SDR achieves comparable runtime to DistR with a modest computational overhead. Additional experimental details are provided in Appendix E. An ablation study on the η hyperparameter has been performed and the results are reported in Appendix F. Since SDR jointly reduces the number of samples, predictive evaluation on held-out data is not directly applicable. Instead, we focus on representation-level properties in these experiments, with predictive performance evaluated separately in Section 5.2 under the context of kernel learning when SDR reduces to a pure DR method.

5.2 Kernel Learning Benchmarks

In this set of experiments, we try to evaluate the effectiveness of SDR as a representation learning method in the context of non-stationary kernel design for GPs. We evaluate on small to medium-sized datasets ($n \leq 2000$) where training flexible, non-stationary GP models can be challenging from an optimization perspective. We focus on this regime where GPs remain practical models, since predictive posterior computation and marginal likelihood evaluation scales as $\mathcal{O}(N^3)$. SDR exhibits the same $\mathcal{O}(N^3)$ scaling in the pure DR setting inheriting this computational complexity directly from the DistR framework.

We test SDR-GP against supervised pure DR methods like neighbour Components Analysis [Goldberger et al., 2004], Supervised UMAP [McInnes et al., 2020] and Kernel Supervised PCA [Barshan et al., 2011] (dubbed as NCA-GP, KSPCA-GP and UMAP-GP respectively). We also compare SDR-GP with DKL and DGP models that are typically considered for non-stationary kernel construction

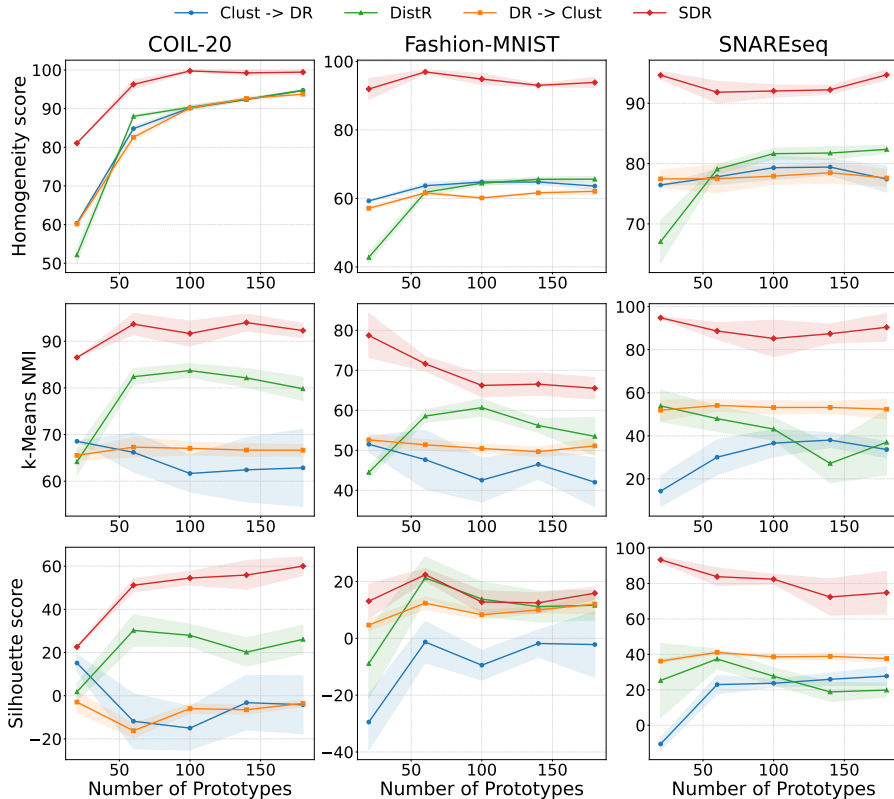


Figure 2: Scores (x100) across varying number of prototypes in \mathbb{R}^2 for all 4 methods.

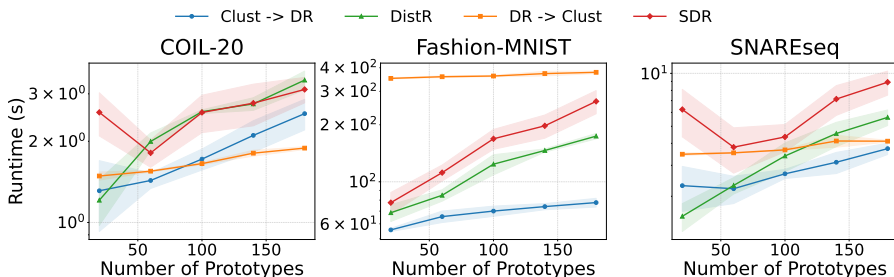


Figure 3: Runtimes across varying number of prototypes in \mathbb{R}^2 for all 4 methods.

in the GP literature. We evaluate these models across three standard UCI benchmark datasets for regression: Boston Housing, Energy Efficiency and Concrete Compressive Strength [Dua and Graff, 2019] along with two image classification benchmark datasets: MNIST [LeCun and Cortes, 2010] and COIL-20 [Nene et al., 1996]. The Mean Log Likelihood (MLL) and the Mean Squared Error (MSE) for the regression tasks are presented in Table 1. The Mean Log Probability (MLP) for the correct class and Accuracy (ACC) for the classification tasks are reported in Table 2. We also test on a variant of DKL that uses pre-trained feature extractor networks in Appendix I.

We evaluate the models not only in terms of predictive performance but also in terms of uncertainty calibration, a key property that makes GPs attractive. Figure 4 shows how the various models behave in terms of predictive performance and uncertainty calibration. While the SDR objective is aimed at improving predictive performance, a GP trained on SDR representations also provides reasonably calibrated uncertainties (more details in Appendix K). The details of the datasets, models and hyperparameters used in these experiments are presented in Appendix H. An ablation study on the β hyperparameter was performed and the results are reported in Appendix J.

	Boston		Energy		Concrete	
	MLL (\uparrow)	MSE (\downarrow)	MLL (\uparrow)	MSE (\downarrow)	MLL (\uparrow)	MSE (\downarrow)
NCA-GP	-0.76 ± 0.31	0.25 ± 0.11	-0.81 ± 0.38	0.29 ± 0.38	-1.01 ± 0.16	0.45 ± 0.12
KSPCA-GP	-0.99 ± 0.27	0.38 ± 0.13	-0.67 ± 0.05	0.22 ± 0.03	-1.28 ± 0.16	0.79 ± 0.23
UMAP-GP	-1.32 ± 0.43	0.39 ± 0.11	-0.53 ± 0.08	0.13 ± 0.06	-1.38 ± 0.19	0.67 ± 0.18
DGP	-1.18 ± 0.09	0.46 ± 0.18	-0.88 ± 0.04	0.12 ± 0.01	-1.10 ± 0.05	0.33 ± 0.06
DKL	-0.42 ± 0.21	0.13 ± 0.07	-0.45 ± 0.03	0.09 ± 0.02	-0.65 ± 0.11	0.21 ± 0.05
SDR-GP (ours)	-0.32 ± 0.18	0.14 ± 0.08	-0.37 ± 0.02	0.05 ± 0.01	-0.40 ± 0.07	0.13 ± 0.02

Table 1: Test results on UCI regression datasets based on five random seeds

	MNIST-2k		COIL-20	
	MLP (\uparrow)	ACC (\uparrow)	MLP (\uparrow)	ACC (\uparrow)
NCA-GP	-0.31 ± 0.04	0.91 ± 0.02	-0.15 ± 0.02	0.98 ± 0.01
KSPCA-GP	-0.46 ± 0.05	0.88 ± 0.02	-0.13 ± 0.02	0.97 ± 0.01
UMAP-GP	-1.05 ± 0.06	0.82 ± 0.00	-0.90 ± 0.22	0.83 ± 0.04
DKL	-0.30 ± 0.05	0.90 ± 0.02	-0.09 ± 0.02	0.99 ± 0.00
SDR-GP (ours)	-0.23 ± 0.02	0.95 ± 0.00	-0.07 ± 0.02	0.99 ± 0.00

Table 2: Test results on image datasets based on five random seeds.

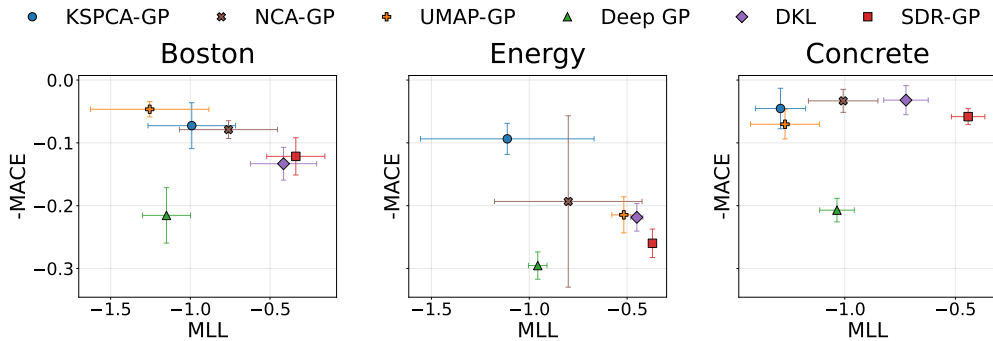


Figure 4: Visualization of different methods depicting the tradeoff between predictive performance in terms of Mean Log Likelihood (MLL) and uncertainty calibration in terms of Mean Absolute Calibration Error (MACE) for the three regression datasets. An ideal model would typically exist in the top-right of this plot which signifies good predictive performance and good uncertainty calibration.

6 Conclusion and Future Work

We introduced Supervised Distributional Reduction (SDR), a framework that integrates optimal transport with dependence maximization to learn compact, target-aware representations. By identifying a supervision bottleneck in FGW and addressing it through a representation-level objective, SDR provides a mechanism for stronger alignment between embeddings and targets while preserving intrinsic data geometry. We further proposed an out-of-sample extension via RKHS projection that provides an explicit transformation map to project unseen points to the embedding space. This allows SDR to be used in predictive pipelines while also regularizing the optimization of the embeddings. Empirical results demonstrate that SDR improves representation quality and yields strong downstream performance, highlighting the effectiveness of combining transport-based structure with explicit supervision. Potential avenues for future work include scaling SDR to larger datasets using low-rank factorizations [Scetbon et al., 2023, Assel et al., 2025], exploring alternative dependence measures [Zhang et al., 2017], and developing more expressive projection operators for the out-of-sample extension. Extending the framework to structured data and leveraging the prototype construction for tasks such as imputation and graph learning are also promising directions.

References

- Hugues Van Assel, Titouan Vayer, Rémi Flamary, and Nicolas Courty. Snekhorn: Dimension reduction with symmetric entropic affinities, 2023. URL <https://arxiv.org/abs/2305.13797>.
- Hugues Van Assel, Cédric Vincent-Cuaz, Nicolas Courty, Rémi Flamary, Pascal Frossard, and Titouan Vayer. Distributional reduction: Unifying dimensionality reduction and clustering with gromov-wasserstein, 2025. URL <https://arxiv.org/abs/2402.02239>.
- Arindam Banerjee, Srujana Merugu, Inderjit S. Dhillon, and Joydeep Ghosh. Clustering with bregman divergences. *J. Mach. Learn. Res.*, 6:1705–1749, December 2005.
- Elnaz Barshan, Ali Ghodsi, Zohreh Azimifar, and Mansoor Zolghadri Jahromi. Supervised principal component analysis: Visualization, classification and regression on subspaces and submanifolds. *Pattern Recognition*, 44(7):1357–1371, 2011. doi: <https://doi.org/10.1016/j.patcog.2010.12.015>. URL <https://www.sciencedirect.com/science/article/pii/S0031320310005819>.
- Edwin V. Bonilla, Kian Ming A. Chai, and Christopher K. I. Williams. Multi-task gaussian process prediction. In *Proceedings of the 21st International Conference on Neural Information Processing Systems*, NIPS’07, pages 153–160, Red Hook, NY, USA, 2007. Curran Associates Inc.
- Song Chen, Blue Lake, and Kun Zhang. High-throughput sequencing of the transcriptome and chromatin accessibility in the same cell. *Nature Biotechnology*, 37, 12 2019. doi: 10.1038/s41587-019-0290-0.
- Youngseog Chung, Ian Char, Han Guo, Jeff Schneider, and Willie Neiswanger. Uncertainty toolbox: an open-source library for assessing, visualizing, and improving uncertainty quantification, 2021. URL <https://arxiv.org/abs/2109.10254>.
- Marco Cuturi and Arnaud Doucet. Fast computation of wasserstein barycenters. In Eric P. Xing and Tony Jebara, editors, *Proceedings of the 31st International Conference on Machine Learning*, volume 32 of *Proceedings of Machine Learning Research*, pages 685–693, Beijing, China, 22–24 Jun 2014. PMLR. URL <https://proceedings.mlr.press/v32/cuturi14.html>.
- Andreas Damianou and Neil D. Lawrence. Deep Gaussian processes. In Carlos M. Carvalho and Pradeep Ravikumar, editors, *Proceedings of the Sixteenth International Conference on Artificial Intelligence and Statistics*, volume 31 of *Proceedings of Machine Learning Research*, pages 207–215, Scottsdale, Arizona, USA, 29 Apr–01 May 2013. PMLR. URL <https://proceedings.mlr.press/v31/damianou13a.html>.
- Dheeru Dua and Casey Graff. UCI machine learning repository, 2019. URL <http://archive.ics.uci.edu/ml>.
- R. A. Fisher. The use of multiple measurements in taxonomic problems. *Annals of Eugenics*, 7(2):179–188, 1936. doi: <https://doi.org/10.1111/j.1469-1809.1936.tb02137.x>. URL <https://onlinelibrary.wiley.com/doi/abs/10.1111/j.1469-1809.1936.tb02137.x>.
- Aden Forrow, Jan-Christian Hütter, Mor Nitzan, Philippe Rigollet, Geoffrey Schiebinger, and Jonathan Weed. Statistical optimal transport via factored couplings. In Kamalika Chaudhuri and Masashi Sugiyama, editors, *Proceedings of the Twenty-Second International Conference on Artificial Intelligence and Statistics*, volume 89 of *Proceedings of Machine Learning Research*, pages 2454–2465. PMLR, 16–18 Apr 2019. URL <https://proceedings.mlr.press/v89/forrow19a.html>.
- Jerome H. Friedman. Multivariate Adaptive Regression Splines. *The Annals of Statistics*, 19(1):1–67, 1991. doi: 10.1214/aos/1176347963. URL <https://doi.org/10.1214/aos/1176347963>.
- Jacob R. Gardner, Geoff Pleiss, David Bindel, Kilian Q. Weinberger, and Andrew Gordon Wilson. Gpytorch: blackbox matrix-matrix gaussian process inference with gpu acceleration. In *Proceedings of the 32nd International Conference on Neural Information Processing Systems*, pages 7587–7597, Red Hook, NY, USA, 2018. Curran Associates Inc.

- Jacob Goldberger, Geoffrey E Hinton, Sam Roweis, and Russ R Salakhutdinov. Neighbourhood components analysis. In L. Saul, Y. Weiss, and L. Bottou, editors, *Advances in Neural Information Processing Systems*, volume 17. MIT Press, 2004. URL https://proceedings.neurips.cc/paper_files/paper/2004/file/42fe880812925e520249e808937738d2-Paper.pdf.
- Arthur Gretton, Kenji Fukumizu, Choon Teo, Le Song, Bernhard Schölkopf, and Alex Smola. A kernel statistical test of independence. In J. Platt, D. Koller, Y. Singer, and S. Roweis, editors, *Advances in Neural Information Processing Systems*, volume 20. Curran Associates, Inc., 2007. URL https://proceedings.neurips.cc/paper_files/paper/2007/file/d5cfead94f5350c12c322b5b664544c1-Paper.pdf.
- Tom Heskes. Bias-variance decompositions: the exclusive privilege of bregman divergences, 2025. URL <https://arxiv.org/abs/2501.18581>.
- Martin Jaggi. Revisiting Frank-Wolfe: Projection-free sparse convex optimization. In Sanjoy Dasgupta and David McAllester, editors, *Proceedings of the 30th International Conference on Machine Learning*, volume 28 of *Proceedings of Machine Learning Research*, pages 427–435, Atlanta, Georgia, USA, 17–19 Jun 2013. PMLR. URL <https://proceedings.mlr.press/v28/jaggi13.html>.
- L. Kantorovitch. On the translocation of masses. *Management Science*, 5(1):1–4, 1958. doi: 10.1287/mnsc.5.1.1. URL <https://doi.org/10.1287/mnsc.5.1.1>.
- Diederik P. Kingma and Jimmy Ba. Adam: A method for stochastic optimization, 2017. URL <https://arxiv.org/abs/1412.6980>.
- Simon Kornblith, Mohammad Norouzi, Honglak Lee, and Geoffrey Hinton. Similarity of neural network representations revisited, 2019. URL <https://arxiv.org/abs/1905.00414>.
- Volodymyr Kuleshov, Nathan Fenner, and Stefano Ermon. Accurate uncertainties for deep learning using calibrated regression. In Jennifer Dy and Andreas Krause, editors, *Proceedings of the 35th International Conference on Machine Learning*, volume 80 of *Proceedings of Machine Learning Research*, pages 2796–2804. PMLR, 10–15 Jul 2018. URL <https://proceedings.mlr.press/v80/kuleshov18a.html>.
- Yann LeCun and Corinna Cortes. MNIST handwritten digit database. <http://yann.lecun.com/exdb/mnist/>, 2010. URL <http://yann.lecun.com/exdb/mnist/>.
- Leland McInnes, John Healy, and James Melville. Umap: Uniform manifold approximation and projection for dimension reduction, 2020. URL <https://arxiv.org/abs/1802.03426>.
- Dimitrios Miliotis, Raffaello Camoriano, Pietro Michiardi, Lorenzo Rosasco, and Maurizio Filippone. Dirichlet-based gaussian processes for large-scale calibrated classification, 2018. URL <https://arxiv.org/abs/1805.10915>.
- Gaspard Monge. *Mémoire sur la théorie des déblais et des remblais*. De l’Imprimerie Royale, 1781.
- Samer A. Nene, Shree K. Nayar, and Hiroshi Murase. Columbia object image library (coil-20). Technical Report CUCS-005-96, Department of Computer Science, Columbia University, February 1996.
- Frank Nielsen and Richard Nock. Sided and symmetrized bregman centroids. *IEEE Transactions on Information Theory*, 55(6):2882–2904, 2009. doi: 10.1109/TIT.2009.2018176.
- Sebastian W. Ober, Carl E. Rasmussen, and Mark van der Wilk. The promises and pitfalls of deep kernel learning, 2021. URL <https://arxiv.org/abs/2102.12108>.
- Michaël Perrot, Nicolas Courty, Rémi Flamary, and Amaury Habrard. Mapping estimation for discrete optimal transport. In D. Lee, M. Sugiyama, U. Luxburg, I. Guyon, and R. Garnett, editors, *Advances in Neural Information Processing Systems*, volume 29. Curran Associates, Inc., 2016. URL https://proceedings.neurips.cc/paper_files/paper/2016/file/26f5bd4aa64fdadf96152ca6e6408068-Paper.pdf.

- Gabriel Peyré, Marco Cuturi, and Justin Solomon. Gromov-wasserstein averaging of kernel and distance matrices. In *Proceedings of the 33rd International Conference on International Conference on Machine Learning - Volume 48*, ICML'16, pages 2664–2672, New York, NY, USA, 2016. JMLR.org.
- Carl Edward Rasmussen and Christopher K. I. Williams. *Gaussian Processes for Machine Learning*. The MIT Press, 11 2005. doi: 10.7551/mitpress/3206.001.0001. URL <https://doi.org/10.7551/mitpress/3206.001.0001>.
- Hugh Salimbeni and Marc Peter Deisenroth. Doubly stochastic variational inference for deep gaussian processes. In *Proceedings of the 31st International Conference on Neural Information Processing Systems*, NIPS'17, pages 4591–4602, Red Hook, NY, USA, 2017. Curran Associates Inc.
- Meyer Scetbon, Gabriel Peyré, and Marco Cuturi. Linear-time gromov wasserstein distances using low rank couplings and costs, 2023. URL <https://arxiv.org/abs/2106.01128>.
- Kevin Tran, Willie Neiswanger, Junwoong Yoon, Qingyang Zhang, Eric Xing, and Zachary W. Ulissi. Methods for comparing uncertainty quantifications for material property predictions, 2020. URL <https://arxiv.org/abs/1912.10066>.
- Laurens van der Maaten and Geoffrey Hinton. Visualizing data using t-sne. *Journal of Machine Learning Research*, 9(86):2579–2605, 2008. URL <http://jmlr.org/papers/v9/vandermaaten08a.html>.
- Titouan Vayer, Nicolas Courty, Romain Tavenard, Laetitia Chapel, and Rémi Flamary. Optimal transport for structured data with application on graphs. In *International Conference on Machine Learning*, 2018. URL <https://api.semanticscholar.org/CorpusID:59523642>.
- Cédric Vincent-Cuaz, Rémi Flamary, Marco Corneli, Titouan Vayer, and Nicolas Courty. Semi-relaxed gromov-wasserstein divergence with applications on graphs, 2022. URL <https://arxiv.org/abs/2110.02753>.
- Kiri Wagstaff, Claire Cardie, Seth Rogers, and Stefan Schrödl. Constrained k-means clustering with background knowledge. In *Proceedings of the Eighteenth International Conference on Machine Learning*, ICML '01, pages 577–584, San Francisco, CA, USA, 2001. Morgan Kaufmann Publishers Inc.
- Kilian Q Weinberger, John Blitzer, and Lawrence Saul. Distance metric learning for large margin nearest neighbor classification. In Y. Weiss, B. Schölkopf, and J. Platt, editors, *Advances in Neural Information Processing Systems*, volume 18. MIT Press, 2005. URL https://proceedings.neurips.cc/paper_files/paper/2005/file/a7f592cef8b130a6967a90617db5681b-Paper.pdf.
- Andrew Gordon Wilson, Zhiting Hu, Ruslan Salakhutdinov, and Eric P. Xing. Deep kernel learning. In Arthur Gretton and Christian C. Robert, editors, *Proceedings of the 19th International Conference on Artificial Intelligence and Statistics*, volume 51 of *Proceedings of Machine Learning Research*, pages 370–378, Cadiz, Spain, 09–11 May 2016. PMLR. URL <https://proceedings.mlr.press/v51/wilson16.html>.
- Han Xiao, Kashif Rasul, and Roland Vollgraf. Fashion-mnist: a novel image dataset for benchmarking machine learning algorithms, 2017. URL <https://arxiv.org/abs/1708.07747>.
- Eric P. Xing, Andrew Y. Ng, Michael I. Jordan, and Stuart Russell. Distance metric learning, with application to clustering with side-information. In *Proceedings of the 16th International Conference on Neural Information Processing Systems*, NIPS'02, pages 521–528, Cambridge, MA, USA, 2002. MIT Press.
- Qinyi Zhang, Sarah Filippi, Arthur Gretton, and Dino Sejdinovic. Large-scale kernel methods for independence testing. *Statistics and Computing*, 28(1):113–130, January 2017. doi: 10.1007/s11222-016-9721-7. URL <http://dx.doi.org/10.1007/s11222-016-9721-7>.

A Proof for Lemma 2 - Optimal Prototype Targets for Bregman Losses

We restate this classical result from Theorem 3.2 in Nielsen and Nock [2009] for the left-sided Bregman centroid (dual form) and Proposition 1 in Banerjee et al. [2005] for the right-sided Bregman centroids (primal form). We provide a self-contained proof in our notation, since the specific form involving the transport coupling T is needed for the elimination argument in Lemma 3.1, the BSGFW objective and Corollary 3.3 that follows.

Case 1 (g_j as first argument - dual form): The definition of a Bregman divergence is given by,

$$D_\phi(g, y_i) = \phi(g) - \phi(y_i) - \langle \nabla \phi(y_i), g - y_i \rangle \quad (12)$$

Consider the supervision loss term,

$$F(g) := \sum_{i=1}^n w_i D_\phi(g, y_i) \quad (13)$$

Expanding the loss term we get,

$$F(g) = \sum_{i=1}^n w_i \phi(g) - \sum_{i=1}^n w_i \phi(y_i) - \sum_{i=1}^n w_i \langle \nabla \phi(y_i), g - y_i \rangle \quad (14)$$

Setting $g = g_j$, $w_i = T_{ij}$, $\sum_{i=1}^n T_{ij} = \pi_j$ we have,

$$F(g_j) = \pi_j \phi(g_j) - \sum_{i=1}^n T_{ij} \phi(y_i) - \langle \sum_{i=1}^n T_{ij} \nabla \phi(y_i), g_j \rangle + \sum_{i=1}^n T_{ij} \langle \nabla \phi(y_i), y_i \rangle \quad (15)$$

Grouping the terms that only depend on g_j we get,

$$F(g_j) = \pi_j \phi(g_j) - \langle \sum_{i=1}^n T_{ij} \nabla \phi(y_i), g_j \rangle + C \quad (16)$$

where C is constant in g_j . Hence minimizing $F(g)$ is equivalent to minimizing

$$G(g_j) = \pi_j \phi(g_j) - \langle \sum_{i=1}^n T_{ij} \nabla \phi(y_i), g_j \rangle \quad (17)$$

Since ϕ is differentiable and strictly convex, G is also differentiable and strictly convex and its unique minimizer is characterized by the first-order condition

$$\nabla G(g_j) = \pi_j \nabla \phi(g_j) - \sum_{i=1}^n T_{ij} \nabla \phi(y_i) = 0 \quad (18)$$

Therefore,

$$\nabla \phi(g_j^*) = \frac{1}{\pi_j} \sum_{i=1}^n T_{ij} \nabla \phi(y_i) \quad (19)$$

Applying $(\nabla \phi)^{-1}$ both sides yields,

$$g_j^* = (\nabla \phi)^{-1} \left(\frac{1}{\pi_j} \sum_{i=1}^n T_{ij} \nabla \phi(y_i) \right) \quad (20)$$

Case 2 (g_j as second argument - primal form): Consider the objective

$$F(g) := \sum_{i=1}^n w_i D_\phi(y_i, g) \quad (21)$$

Expanding the objective we get,

$$F(g) = \sum_{i=1}^n w_i \phi(y_i) - \sum_{i=1}^n w_i \phi(g) - \sum_{i=1}^n w_i \langle \nabla \phi(g), y_i - g \rangle \quad (22)$$

Setting $g = g_j$, $w_i = T_{ij}$, $\sum_{i=1}^n T_{ij} = \pi_j$ we have,

$$F(g_j) = \sum_{i=1}^n T_{ij} \phi(y_i) - \pi_j \phi(g_j) - \langle \nabla \phi(g_j), \sum_{i=1}^n T_{ij} y_i - \pi_j g_j \rangle \quad (23)$$

Using the definition of \bar{y} (weighted average of the targets), given by $\sum_{i=1}^n T_{ij} y_i = \pi_j \bar{y}$, we get

$$F(g_j) = \sum_{i=1}^n T_{ij} \phi(y_i) - \pi_j \phi(g_j) - \pi_j \langle \nabla \phi(g_j), \bar{y} - g_j \rangle \quad (24)$$

$$= \sum_{i=1}^n T_{ij} \phi(y_i) + \pi_j (-\phi(g_j) - \langle \nabla \phi(g_j), \bar{y} - g_j \rangle) \quad (25)$$

$$= \sum_{i=1}^n T_{ij} \phi(y_i) - \pi_j \phi(\bar{y}) + \pi_j (\phi(\bar{y}) - \phi(g_j) - \langle \nabla \phi(g_j), \bar{y} - g_j \rangle) \quad (26)$$

Recognizing the Bregman Divergence in the last term

$$F(g_j) = \sum_{i=1}^n T_{ij} \phi(y_i) - \pi_j \phi(\bar{y}) + \pi_j D_\phi(\bar{y}, g_j) \quad (27)$$

The first two terms do not depend on g_j . Therefore minimizing $F(g_j)$ over g_j is equivalent to minimizing $D_\phi(\bar{y}, g_j)$. Since $D_\phi(\bar{y}, g_j) \geq 0$ for all $g \in \mathcal{G}$, with equality iff $g = \bar{y}$ (by strict convexity of ϕ), the unique minimizer is

$$g_j^* = \bar{y} \quad (28)$$

Hence, the optimal prototype targets are given by the expression

$$g_j^* = \frac{1}{\pi_j} \sum_{i=1}^n T_{ij} y_i \quad (29)$$

B Closed form expression for optimal prototype targets

B.1 $L_s \rightarrow$ L2-loss

We can make use of Lemma 2 to derive the optimal prototype targets when L_s is the L2-loss. The L2-loss is symmetric w.r.t to the targets and prototype targets and so it does not really make a difference on which case of Lemma 2 we employ to arrive at the expression for g_j^* . In this case, we will just use Case 1 of Lemma 2 assuming g_j is the first argument of the L_s loss function. For L2-loss we have

$$\phi(y) = \frac{1}{2} \|y\|_2^2 \quad (30)$$

The gradient of ϕ is then given by,

$$\nabla \phi(y) = y \quad (31)$$

$$\Rightarrow (\nabla \phi)^{-1}(y) = y \quad (32)$$

Lemma 2 then gives,

$$g_j^*(T) = (\nabla \phi)^{-1} \left(\frac{1}{\pi_j} \sum_{i=1}^n T_{ij} \nabla \phi(y_i) \right) \quad (33)$$

$$= \frac{1}{\pi_j} \sum_{i=1}^n T_{ij} y_i \quad (34)$$

This just means that the prototype targets are nothing but a weighted sum of all targets weighted according to the coupling matrix T .

B.2 $L_s \rightarrow$ Cross-Entropy Loss

The modified Cross-Entropy (CE) loss as described in Heskes [2025] is given by

$$L_s(y, g) = \sum_{k=1}^c y_k \log \left(\frac{y_k}{g_k} \right) + \sum_{k=1}^c g_k - \sum_{k=1}^c y_k \quad (\text{Modified CE-Loss})$$

The modified CE loss is a valid Bregman divergence with the following generator function

$$\phi(u) = \sum_{k=1}^c u_k \log u_k - \sum_{k=1}^c u_k \quad (35)$$

The modified CE loss takes g as the second argument and thus Case 2 of Lemma 2 applies. As a direct consequence, the optimal prototype targets are given by

$$g_j^* = \frac{1}{\pi_j} \sum_{i=1}^n T_{ij} y_i \quad (36)$$

This means that the prototypes in the embedding space carry soft class labels unlike the points in the input space which might have hard labels when one-hot encoded.

Note: The result established above is general and applies when the domain of g is extended from the probability simplex Δ^{c-1} to the unit cube $[0, 1]^c$ i.e even when we ignore the simplex normalization constraint $\sum_{k=1}^c g_k = 1$. In the case where y is a (one-hot encoded) label vector and g satisfies the simplex normalization constraint, the modified CE loss collapses to the classic CE loss.

C FGW Supervision Bottleneck

C.1 Mathematical intuition for the Supervision Bottleneck

In this section, we provide some mathematical intuition into the observation made in Remark 3.4. Recall the partially minimized BS-FGW objective,

$$\mathcal{J}(T, Z) = (1 - \alpha)S(T) + \alpha GW(T; Z) \quad (37)$$

where $S(T)$ is the supervision loss term defined as,

$$S(T) = \sum_{i=1}^n \sum_{j=1}^m L_s(y_i, g_j^*(T)) T_{ij} \quad (38)$$

For part (i), observe that once the prototype targets $g_j^*(T)$ are replaced with the closed forms from Lemma 2, the supervised term $S(T)$ depends only on the coupling matrix T and not explicitly on Z . Therefore, for fixed T ,

$$\nabla_Z S(T) = 0 \quad (39)$$

So the Z -update is governed only by the geometric term $\alpha GW(Z; T)$. This establishes that supervision does not directly act on the representation updates.

For Part (ii), let $T^*(Z)$ denote the optimal coupling as a function of Z , assuming this solution map is locally differentiable. Then the supervised term becomes the composite map

$$Z \mapsto T^*(Z) \mapsto S(T^*(Z)) \quad (40)$$

Applying the chain rule gives,

$$\nabla_Z S(T^*(Z)) = \left(\frac{\partial T^*(Z)}{\partial Z} \right)^T \nabla_T S(T^*(Z)) \quad (41)$$

Taking norms on both sides and using the standard operator norm bound $\|Av\| \leq \|A\| \|v\|$ we obtain,

$$\|\nabla_Z S(T^*(Z))\| \leq \left\| \frac{\partial T^*(Z)}{\partial Z} \right\| \|\nabla_T S(T^*(Z))\| \quad (42)$$

Hence, the supervised gradient reaching Z is modulated by the sensitivity of the optimal coupling to perturbations in the embedding. In particular, if $T^*(Z)$ is locally insensitive to Z or if $T^*(Z)$ is dominated by structural constraints, then the supervised signal on Z is attenuated potentially leading to a very weak alignment between the embeddings Z and the targets Y .

C.2 Empirical Evidence for the Supervision Bottleneck and the Effect of Explicit Dependence Maximization in SDR

In this study, we provide empirical evidence for the supervision bottleneck and why an explicit dependence maximization term is required for Supervised Distributional Reduction to work. The FGW-only version is where the BSFGW objective is used for optimizing both \mathbf{T} and \mathbf{Z} with the BCD algorithm. We compare this approach with the SDR objective that includes an explicit dependence maximization term in the form of CKA. We report the CKA scores and the Silhouette scores for the FGW-only and the SDR variants in Table 3 for the COIL-20 and SNAREseq datasets. We can see that the CKA score of the FGW-only objective is worse than the score of the original dataset. This shows that the FGW-only objective dilutes the supervision signal and that the embeddings optimize for other desirable properties like structural alignment. We observe that FGW-only fails to preserve representation-target dependence, as evidenced by lower CKA scores and worse geometric separation (silhouette score). In contrast, SDR significantly improves both metrics, indicating that supervision mediated solely through the coupling matrix is insufficient and that explicit dependence maximization is necessary to learn target-aligned representations.

Plots (a) and (b) in Figure 5 show how the CKA score of the embeddings Z with respect to the targets evolve in the first inner loop of the SDR objective. This inner loop corresponds to the optimization of Z using an Adam optimizer and runs at most for 1000 steps. Plots (c) and (d) show how the CKA score progresses with the outer loop which consists of two steps: an inner loop for optimizing Z and a solve of the srBSFGW objective to update the coupling matrix T . We can clearly see that the FGW objective plateaus and produces a worse CKA score than the actual data whereas the SDR objective

	COIL-20 ($m = 200$)		SNAREseq ($m = 200$)	
	CKA Score (\uparrow)	Silhouette Score (\uparrow)	CKA Score (\uparrow)	Silhouette Score (\uparrow)
Original Data	0.48	-	0.45	-
FGW-only	0.31 ± 0.03	26.96 ± 6.19	0.38 ± 0.04	6.19 ± 4.08
SDR	0.56 ± 0.02	58.93 ± 2.70	0.91 ± 0.02	64.13 ± 9.72

Table 3: CKA and Silhouette Score comparison for pure FGW and SDR objectives across 5 seeds

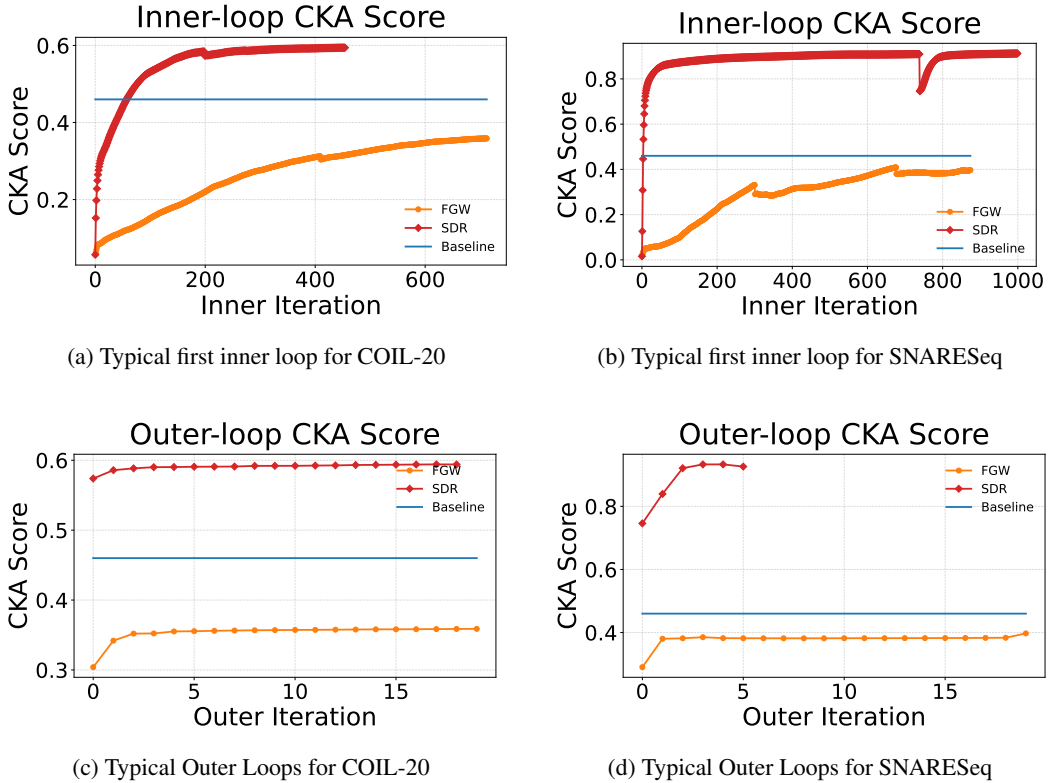


Figure 5: Variation of the CKA score across inner and outer loops of the optimization process for COIL20 and SNARESeq datasets.

produces a high CKA score that indicates the retention of predictive signal leading to target-aware embeddings.

Figure 6 shows example embeddings generated by SDR and the FGW-only variant for the COIL-20 and SNAREseq datasets. SDR produces reasonably well separated clusters of the different classes in the dataset whereas the FGW-only variant although manages to bring prototypes from the same class together does not form well separated clusters. This shows that the FGW extension is useful but the dependence maximization term in the SDR objective makes it more effective in capturing the nuances of the dataset.

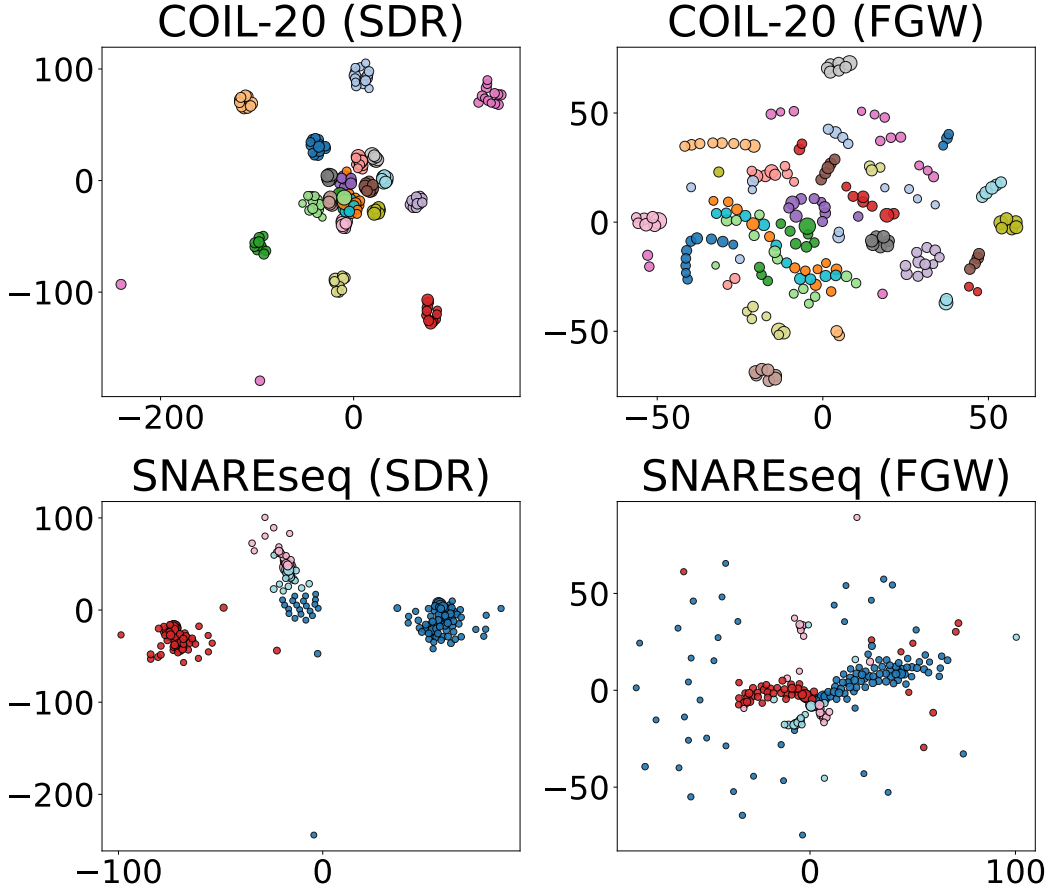


Figure 6: Example embeddings for the COIL20 and SNAREseq datasets for the SDR and FGW-only objectives for visual comparison.

D Code/Implementation details

The implementation of SDR was built on top of the DistR¹ implementation from Assel et al. [2025]. The benchmarking scripts for kernel learning use GP models constructed with GPyTorch²[Gardner et al., 2018]. For solving the srBSFGW objective, we use the FGW/semi-relaxed FGW solvers from the Python Optimal Transport (POT)³ library. All experiments were implemented in Python using PyTorch for automatic differentiation and GPU acceleration. Experiments were run on NVIDIA GPUs; the distributional reduction benchmarks used an NVIDIA L4 GPU, while the kernel learning benchmarks used an NVIDIA A100-80GB GPU. All reported means and standard deviations (1-sigma error bars) are computed over multiple random seeds, with the number of seeds specified in the corresponding experimental section.

¹<https://github.com/huguesva/Distributional-Reduction>

²<https://docs.gpytorch.ai/en/stable/>

³<https://pythonot.github.io>

E Distributional Reduction Experimental Details

E.1 Datasets

The experiments for distributional reduction (joint clustering and DR) used three datasets with varying properties. We use the COIL-20 [Nene et al., 1996], Fashion MNIST [Xiao et al., 2017] and SNAREseq [Chen et al., 2019] datasets for all distributional reduction experiments. The details of these datasets are provided in Table 4.

Dataset	Number of Points	Input Features	Number of Classes
COIL-20	1440	16384	20
Fashion-MNIST	10000	784	10
SNAREseq (Chromatin)	1047	19	4

Table 4: Details of Datasets used in Distributional Reduction experiments

COIL-20 and the Fashion-MNIST datasets were pre-processed with PCA to reduce the number of features to 50 as done in practice (Assel et al. [2025], van der Maaten and Hinton [2008]) and the inputs were normalized for all three datasets.

E.2 Experiments

The distributional reduction experiments were performed on 3 different datasets as mentioned in the previous sub-section. The methods tested were DistR, Cluster-then-DR and DR-then-Cluster following the same experimental setup in Assel et al. [2025]. The experiments were run for different number of prototypes {20, 60, 100, 140, 180} with 5 random seeds. For evaluation metrics, we consider the Homogeneity score, k-means Normalized Mutual Information and the Silhouette Score as defined in Assel et al. [2025]. All experiments were run on a remote server equipped with an NVIDIA-L4 GPU.

E.3 Hyperparameter settings

All steps involving clustering both for the initialization of the coupling matrices and for methods that explicitly perform clustering, the Spectral Clustering implementation from scikit-learn was used. For all experiments, DistR and SDR used the Symmetric Entropic Affinity [Assel et al., 2023] for \mathbf{X} with the perplexity hyperparameter tuned between {20, 30, 50, 100, 200} and the learning rate tuned between {0.01, 0.1, 1.0}. The learning rates were chosen as the highest value in the set that did not break the optimization routine of the SEA transport problem. We report these tuned values for the various datasets in Table 5.

Dataset	Perplexity	Learning Rate
COIL-20	20	0.1
Fashion-MNIST	50	0.01
SNAREseq (Chromatin)	30	0.01

Table 5: Hyperparameter details of SEA for various datasets

For the embeddings \mathbf{Z} , the normalized Student-t affinity [van der Maaten and Hinton, 2008] was used. For the CKA computation, we require positive semi-definite kernels and so affinities cannot be directly used. Therefore, we choose the kernel that is closest in behaviour to the normalized Student-t affinity which is the Rational Quadratic (RQ) kernel [Rasmussen and Williams, 2005] given by

$$k_{RQ}(x, x') = \left(1 + \frac{\|x - x'\|^2}{2\alpha l^2}\right)^{-\alpha} \tag{43}$$

This kernel is equivalent to adding several SE kernels with different lengthscales parameters. The parameter α determines how large scale variations are weighted relative to small scale variations.

The RQ kernel behaves like a heavy-tailed similarity function since it decays polynomially. Since, all the datasets used in these experiments are classification datasets, we use the delta kernel for the outputs as described in Barshan et al. [2011]. For all experiments, α in the srBSFGW objective was set to 0.2 and η in the SDR objective was set to 1000. The Adam optimizer was used for updating the embeddings Z with the default learning rate of 0.001.

F Ablation study (η): Effect of Dependence Strength

η is a very important hyperparameter that determines the influence of the targets in the optimization process of the embeddings Z according to the SDR objective. In this section, we present some results on the ablation of the η parameter. Since the CKA term is a normalized version of the HSIC loss it always lies in $[0, 1]$. Therefore, depending on the magnitude of the GW loss η can be suitably tuned. We sweep across η in the log space and for three different number of prototypes $\{20, 100, 180\}$. The results for the COIL-20 and SNAREseq datasets are presented in 7 and 8 respectively. For most of the cases in Figure 7 and Figure 8, it is evident that a higher η value improves the quality of the embeddings produced by SDR. However, we can observe diminishing gains in the quality of the embeddings in many of these plots after a value of 10^3 for η . Also, for the DKL experiments there was a trade-off that we observed between how well the OOS map L can approximate a very complex map produced by SDR through OT and maximizing predictive signal in the prototypes. So, a reasonably high value of η produces high-quality prototypes and the value we chose for all our experiments was 10^3 .

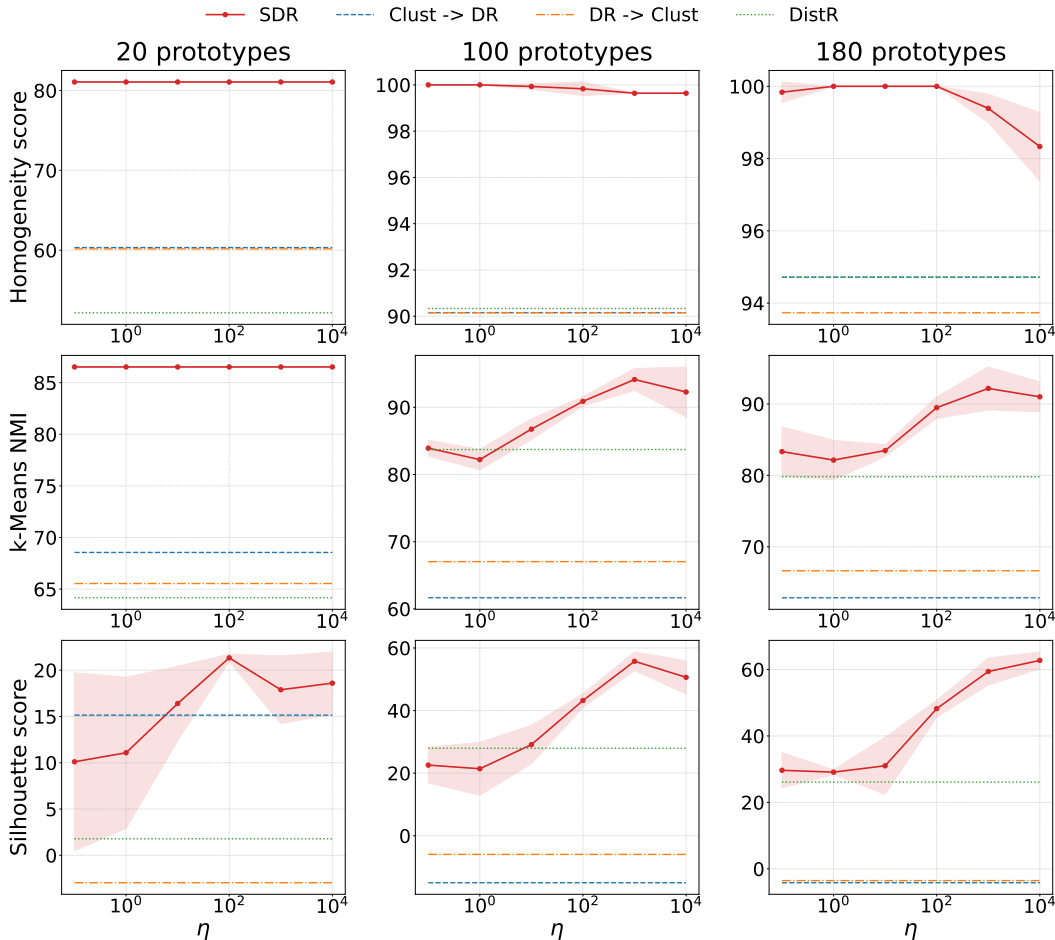


Figure 7: Scores (x100) across varying values of η for the COIL-20 dataset averaged over three random seeds. The flat lines show the average performance of the other methods as a baseline for comparison for a given number of prototypes.

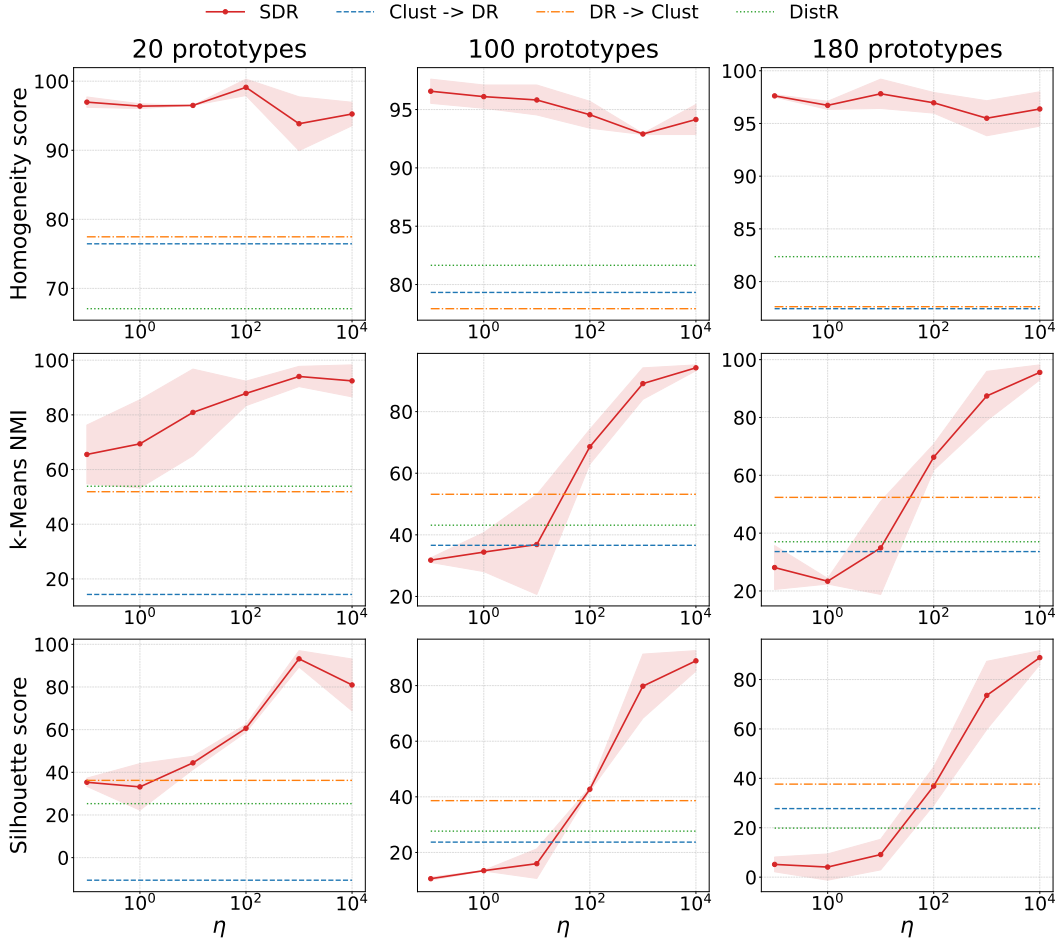


Figure 8: Scores (x100) across varying values of η for the SNAREseq dataset averaged over three random seeds. The flat lines show the average performance of the other methods as a baseline for comparison for a given number of prototypes.

G Additional DR Visualizations and Downstream Evaluation

SDR just like DistR inherits the same runtime complexity $\mathcal{O}(n^2m + nm^2)$ where n is the number of source samples and m is the number of target samples. For the pure DR case ($p < d, n = m$), SDR scales as $\mathcal{O}(n^3)$. This is one of the core reasons why SDR is feasible as a distributional reduction method but not very scalable as a DR method. However, SDR might still be a very useful DR method in the low-data regime. While this is evident from the experiments in Section 5.2, we show visualizations of two toy datasets namely: (i) S-curve and (ii) Swiss Roll datasets to show how SDR behaves as a DR method when compared with other supervised DR methods. We chose these datasets, since they are the most basic datasets tested for every DR method and is easier to visualize the embeddings along with the original data since the original data lives in 3D. We compare the embeddings generated from Supervised-UMAP (S-UMAP) and Kernel Supervised PCA (KS-PCA) visually. For the S-curve dataset, we set the number of neighbours to 50 and for the swiss roll dataset we set this parameter to 20 to generate the supervised UMAP visualizations. For SDR, we choose the exact same settings used in the kernel learning experiments. The expected behaviour for any DR method on these two datasets is to unroll the curves onto flat rectangular strips in the 2D space. We can see that SDR achieves this quite cleanly compared to S-UMAP or KS-PCA. Along with this we also use the Friedman dataset [Friedman, 1991] for testing models on a downstream predictive task. We test the predictive performance of a k-Nearest Neighbours (k-NN) model and a Kernel Ridge Regression (KRR) model to show that the SDR embeddings work well in a model-agnostic manner.

We report the R^2 scores for this experiment in Tables 6 and 7 and the metrics reported are across 5 different random seeds.

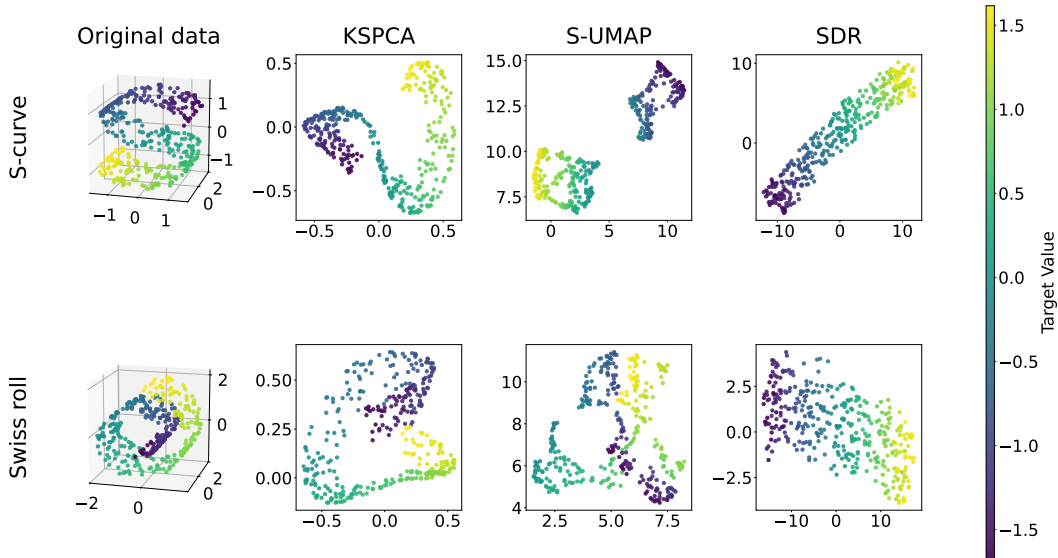


Figure 9: Visualizing embeddings in the pure DR setting for KSPCA, (S-UMAP) and SDR on toy 3D datasets.

	S-curve (100 points)		Swiss Roll (100 points)		Friedman (500 points)	
	Train	Test	Train	Test	Train	Test
Supervised UMAP	0.99 ± 0.00	0.88 ± 0.08	0.99 ± 0.00	0.47 ± 0.49	0.99 ± 0.00	0.51 ± 0.14
KS-PCA	0.92 ± 0.06	0.93 ± 0.05	0.89 ± 0.10	0.85 ± 0.10	0.81 ± 0.02	0.71 ± 0.10
SDR	0.97 ± 0.02	0.94 ± 0.06	0.99 ± 0.01	0.97 ± 0.03	0.98 ± 0.00	0.91 ± 0.03

Table 6: R^2 scores for k-NN Regressor with $k = 10$.

	S-curve (100 points)		Swiss Roll (100 points)		Friedman (500 points)	
	Train	Test	Train	Test	Train	Test
Supervised UMAP	0.97 ± 0.01	0.82 ± 0.13	0.98 ± 0.01	0.53 ± 0.34	0.98 ± 0.00	0.55 ± 0.12
KS-PCA	0.90 ± 0.06	0.92 ± 0.06	0.86 ± 0.12	0.82 ± 0.12	0.80 ± 0.03	0.72 ± 0.08
SDR	0.98 ± 0.01	0.96 ± 0.03	0.99 ± 0.01	0.96 ± 0.05	0.98 ± 0.00	0.91 ± 0.02

Table 7: R^2 scores for KRR Regressor with $\alpha = 1$ (lengthscale of RBF kernel).

In several cases, SDR is better than Supervised UMAP on the test R^2 scores and is comparable on the train R^2 scores. This also shows that the mechanism of optimizing for L not only provides a mechanism to project OOS points onto the embedding space but also regularizes the optimized embeddings Z resulting in better test performance for a downstream predictor.

H Kernel Learning Experimental Details

H.1 Datasets

The experiments comparing SDR-GP with all the other methods included 5 datasets where 3 of them are regression datasets sourced from the UCI repository and 2 of them are classification datasets. The details of these datasets are provided in Tables 8 and 9.

Dataset	Number of Points	Input Features	Output Features
Boston Housing	506	13	1
Energy Efficiency	768	8	2
Concrete Compressive Strength	1030	8	1

Table 8: Details of Regression Datasets used in Kernel Learning experiments

Dataset	Number of Points	Input Features	Number of Classes
MNIST	2000	784 (28×28)	10
COIL-20	1440	16384 (128×128)	20

Table 9: Details of Classification (Image) Datasets used in Kernel Learning experiments

H.2 Models

We compare 5 different models in this experiment. We compare SDR-GP against Deep Kernel Learning [Wilson et al., 2016] and Deep Gaussian Processes (Damianou and Lawrence [2013], Salimbeni and Deisenroth [2017]) which are the most natural ways to add non-stationarity to GPs for modelling non-smooth functions. Since SDR also acts as a pure DR method in this application, we compare against two other supervised DR methods namely Kernel Supervised PCA [Barshan et al., 2011] and Supervised UMAP [McInnes et al., 2020] that act as embedding models/feature extractors for the GP. We dub these models KSPCA-GP and UMAP-GP respectively. For KSPCA, we use RBF kernels for the inputs, RBF and Delta kernels on the targets for regression and classification datasets respectively. For supervised UMAP, we use the official UMAP⁴ library. We set the number of neighbours to 50, the effective minimum distance between embedded points to 0.1 and the distance metric to 'L2'.

H.3 NN architectures and GP settings

For regression tasks, we use the same NN Feature Extractor which is just a Multilayer-Perceptron network with ReLU activations used in Wilson et al. [2016]. This is a fully connected DNN with [d-1000-500-50-2] architecture. The GP for the Boston and the Concrete datasets are exact GPs that use an RBF kernel with Automatic Relevance Determination (ARD) [Rasmussen and Williams, 2005] and the standard Gaussian likelihood. The GP for the Energy dataset is a multi-task GP [Bonilla et al., 2007] that models both the covariances between the inputs and the output tasks with an RBF kernel (equipped with ARD) and a Gaussian likelihood.

The Deep GP model was constructed with one hidden layer and an output layer. The latent dimensions of the hidden layer were set to match the latent dimensions of all the other models. This model is trained variationally using the doubly stochastic variational inference technique described by Salimbeni and Deisenroth [2017]. The number of inducing points is set to 128 and the number of likelihood samples is set to 16.

For the classification tasks, we again use the same CNN feature extractor described in [Wilson et al., 2016] (Appendix A.1 in the paper). However, we use this feature extractor for classification instead of orientation extraction as described in the DKL paper. We use an exact GP with a Dirichlet likelihood for multi-class classification inspired by the work of Milios et al. [2018]. We set α_ϵ (concentration parameter of the Dirichlet likelihood) to 0.01 and the number of samples from the GP posterior to 256 since the posterior predictions cannot be obtained in closed form and needs to be MC-sampled.

⁴<https://umap-learn.readthedocs.io/en/latest/index.html>

H.4 SDR settings

For SDR, we use the Symmetric Entropic Affinity(SEA) from Assel et al. [2023] on the inputs \mathbf{X} for all experiments in this section with the perplexity and the learning rate tuned for each dataset. The perplexity value was set to 20 for all experiments. The learning rate parameter was set to 0.01 for the regression datasets and 0.1 for the image datasets. The normalized Student-t affinity was used to compute affinities for the embeddings \mathbf{Z} . For the HSIC computation, we use the Rational Quadratic (RQ) kernel for the embedding space and the RBF/Delta kernel [Barshan et al., 2011] for the regression/classification outputs. The kernel \mathbf{K} in the SDR-OOS objective is computed with RBF for all the experiments. The α parameter in the srBSFGW objective is set to 0.2, η is set to 1000, β is set to 0.5 and λ_L was set to $1e - 2$ for all experiments. The initialization of the coupling matrix \mathbf{T} is done using Spectral clustering for regression tasks. \mathbf{T} is initialized randomly for classification tasks since any clustering technique can run into the issue of producing degenerate clusters when the number of clusters required is much higher than the number of actual clusters present in the data which is typically the case with classification and the pure DR setting.

H.5 Experimental Details

For the regression datasets, the number of embedding dimensions was set to 2 and for the classification datasets the number of embedding dimensions was set to 10 following the practice in Ober et al. [2021]. All the GP models were trained for 20 epochs for the regression benchmarks and were trained for 50 epochs for the classification benchmarks. The learning rate was set to 0.1 for all the models. The test data size was set to 0.2 for all experiments. We were unable to obtain stable DGP results within our compute budget for the classification setting due to memory pressure when scaling the number of latent dimensions to 10. This experiment was run on a remote server equipped with an NVIDIA A100-80GB GPU so that the Dirichlet GP fits in memory for the image classification datasets.

H.6 Model training times

We report the training times for the various models that were considered for the kernel learning benchmarks (Section 5.2) in Table 10. The training times reported for KSPCA-GP, UMAP-GP and SDR-GP includes the time taken to fit the DR transform and the time taken to train the GP since the fitting of the DR transform is decoupled from GP training in these models.

	Boston	Energy	Concrete	COIL-20	MNIST-2k
NCA-GP	0.45 ± 0.07	1.34 ± 0.30	3.00 ± 1.20	1.76 ± 0.13	2.62 ± 0.24
KSPCA-GP	0.15 ± 0.08	0.61 ± 0.01	0.49 ± 0.05	1.27 ± 0.04	1.09 ± 0.03
UMAP-GP	8.01 ± 16.42	1.70 ± 0.05	1.93 ± 0.15	16.59 ± 12.10	6.80 ± 0.10
DGP	0.44 ± 0.07	0.80 ± 0.01	0.41 ± 0.00	-	-
DKL	0.53 ± 0.89	0.56 ± 0.02	0.39 ± 0.03	34.63 ± 0.31	2.40 ± 0.06
SDR-GP (ours)	7.07 ± 2.21	5.14 ± 0.60	8.42 ± 2.44	8.00 ± 0.57	17.47 ± 2.55

Table 10: Runtime (in seconds) for all datasets based on five random seeds

I Comparison with pre-trained feature extractors for DKL

A widely used variant of DKL is where the feature extractor networks are pre-trained and then fine-tuned jointly along with the GP hyperparameters instead of training them from scratch. We use the same networks used for the experiments in Section 5.2 but pre-train them using squared loss and cross-entropy loss for the regression and classification benchmarks respectively. We train them during the pre-training phase for 75 epochs and with a learning rate of $1e - 3$ followed by a training phase of 20 epochs for the regression datasets and 50 epochs for the classification datasets with a learning rate of 0.01. The results are show in Tables 11 and 12 where DKL-joint corresponds to the model where the NN feature extractor is trained from scratch jointly with the GP hyperparameters

and DKL-pretrained corresponds to the model where the NN feature extractor is pre-trained and then fine-tuned along with the GP hyperparameters in the joint-training phase.

	Boston		Energy		Concrete	
	MLL (\uparrow)	MSE (\downarrow)	MLL (\uparrow)	MSE (\downarrow)	MLL (\uparrow)	MSE (\downarrow)
DKL-joint	-0.42 ± 0.21	0.13 ± 0.07	-0.45 ± 0.03	0.09 ± 0.02	-0.65 ± 0.11	0.21 ± 0.05
DKL-pretrained	-0.76 ± 0.05	0.11 ± 0.07	-0.71 ± 0.10	0.08 ± 0.02	-0.82 ± 0.01	0.17 ± 0.01
SDR-GP (ours)	-0.32 ± 0.18	0.14 ± 0.08	-0.37 ± 0.02	0.05 ± 0.01	-0.40 ± 0.07	0.13 ± 0.02

Table 11: Test results for DKL variants on UCI regression datasets based on five random seeds

	MNIST-2k		COIL-20	
	MLP (\uparrow)	ACC (\uparrow)	MLP (\uparrow)	ACC (\uparrow)
DKL-joint	-0.30 ± 0.05	0.90 ± 0.02	-0.09 ± 0.02	0.99 ± 0.00
DKL-pretrained	-0.25 ± 0.10	0.94 ± 0.03	-0.13 ± 0.01	0.97 ± 0.03
SDR-GP (ours)	-0.23 ± 0.02	0.95 ± 0.00	-0.07 ± 0.02	0.99 ± 0.00

Table 12: Test results for DKL variants on image classification datasets based on five random seeds.

These results emphasise that the performance of improvements of SDR are not solely attributable to the joint feature learning regime of DKL. Even in this controlled setting where both SDR and DKL operate on comparable pretrained features, SDR consistently achieves comparable or better predictive performances. These results suggest that the observed gains arise from the proposed SDR formulation itself rather than differences in representation learning or end-to-end optimization dynamics.

J Ablation study (β): Effect of Projection Regularization

The hyperparameter β used in the SDR-OOS objective for the intermediate projection of the embeddings Z plays a key role in defining the predictive performance of the downstream model. β handles the trade-off of the embeddings being representable by a projection map against the retention of predictive signal in the optimized embeddings. In this experiment, we ran a sweep over the range of β . The range of β is $[0, 1]$. $\beta = 0$ corresponds to no regularization of Z with respect to L and $\beta = 1$ tries to replace the optimized Z in an iteration with its projection onto the RKHS representable set of K . We sample β at uniform intervals in this range which corresponds to $\{0.0, 0.25, 0.5, 0.75, 1.0\}$ and run the SDR-GP method on all three regression datasets. From the plots it is evident that a high β value improves the test error by pulling the optimized Z back onto the RKHS representable set of K . However, this can potentially misalign Z with targets Y to some degree and this manifests as increasing training error. On the other hand, a low β value improves the training error but increases the test error since the optimization of Z is now less regularized. To maintain a balance between these competing factors, a value close to the mean/median of this range which is 0.5 seems to be a sensible choice for this parameter and this is the value we use across all the other experiments. We ran this experiment across 3 different random seeds and the mean is reported in the various plots of Figure 10.

Additionally, the behavior observed across the β sweep highlights the role of the SDR regularization term as an implicit complexity control mechanism on the learned embeddings. The relatively stable performance observed around intermediate β values further suggests that SDR-GP is not overly sensitive to precise tuning of this parameter, indicating robustness of the proposed objective across a reasonably broad operating regime. This behavior is consistent across all evaluated datasets and supports the interpretation of β as governing a bias-variance trade-off between representability and predictive alignment of the optimized embeddings.

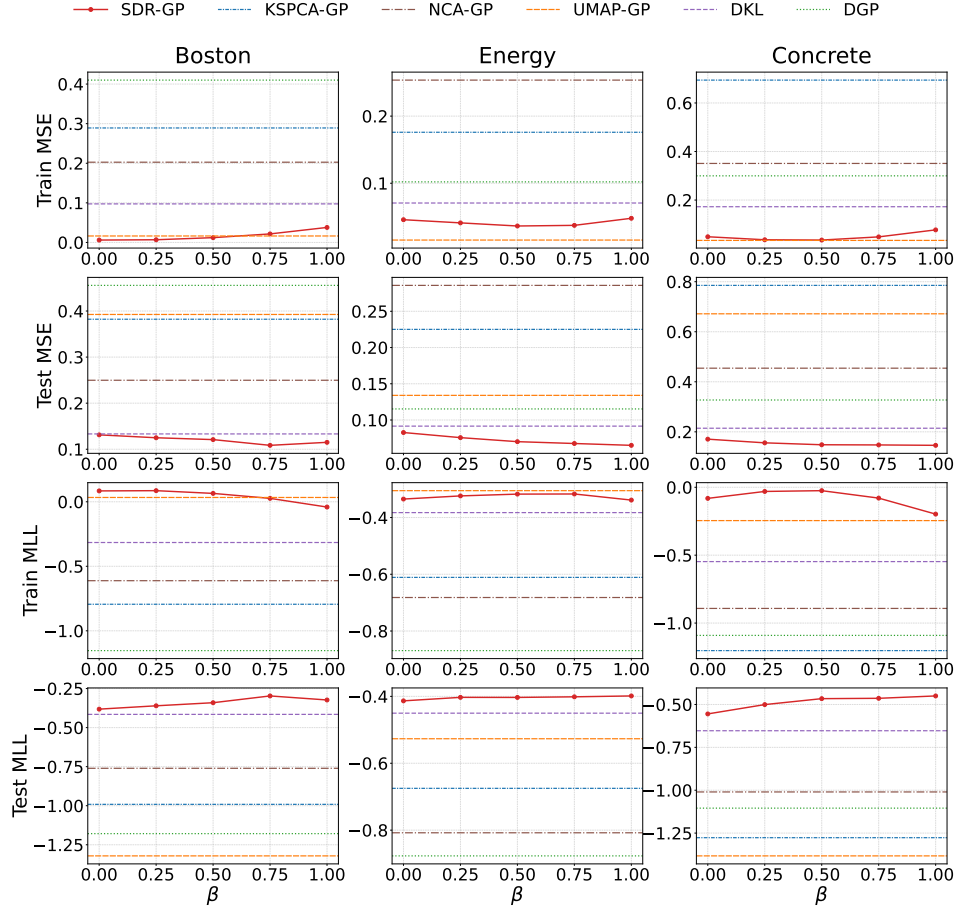


Figure 10: Ablation on the β parameter for the regression datasets. A very high β value (close to 1) increases training error but improves the test error. A low β value (close to 0) decreases the training error but increases the test error. The dashed lines corresponds to the baseline performance of other methods.

K Uncertainty Calibration Diagnostics

When assessing probabilistic ML models, uncertainty calibration plays a major role in analyzing the predictive uncertainties produced by a model. For this, we use standard calibration curves and Mean Absolute Calibration Error as the metric. Figure 11 shows typical calibration curves of all the models in our experimental suite for the UCI regression datasets.

A calibration curve fundamentally validates the fact: **"An $\alpha\%$ prediction interval should contain $\alpha\%$ of the true values"**. For a scalar metric, we compute MACE following the uncertainty-toolbox convention of Chung et al. [2021], based on the regression calibration framework of Kuleshov et al. [2018]. For Gaussian predictive uncertainties, this corresponds to comparing nominal Gaussian interval/quantile probabilities with empirical coverage, as in Tran et al. [2020]. In this work, we stick to the symmetric interval calibration mode for generating the calibration curves. The number of levels across which we assess the calibration is set to $n_{bins} = 99$. For $n_{bins} = 99$, we consider uniformly spaced confidence intervals $\alpha_k \in (0, 1)$. The "Interval" mode constructs symmetric prediction bands as follows:

$$[\hat{y} - z_{\alpha_k} \hat{\sigma}, \hat{y} + z_{\alpha_k} \hat{\sigma}], z_{\alpha_k} = \Phi^{-1} \left(\frac{1 + \alpha_k}{2} \right) \quad (44)$$

where \hat{y} is the predicted mean, $\hat{\sigma}$ is the predicted standard deviation and Φ^{-1} is the inverse CDF of a Gaussian distribution.

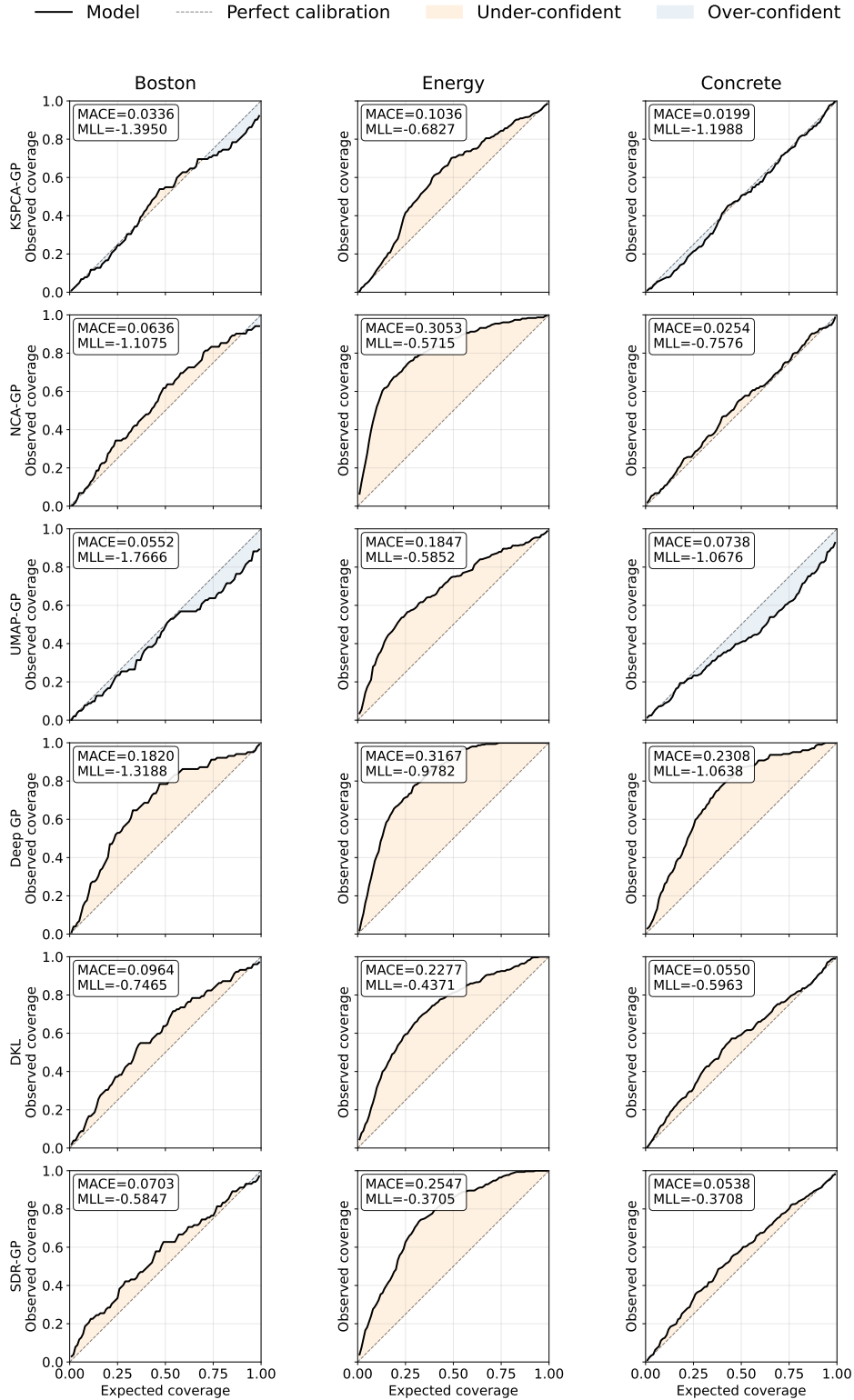


Figure 11: Calibration curves for the UCI regression datasets. The dotted diagonal line is the ideal calibration curve. Anything above the diagonal means the model is under-confident and anything below the diagonal means the model is over-confident.